

Critical behavior and magnetocaloric effect in VI_3

Yu Liu and C. Petrovic

*Condensed Matter Physics and Materials Science Department,
Brookhaven National Laboratory, Upton, New York 11973, USA*

(Dated: March 14, 2019)

We investigated critical properties and magnetocaloric effect connected with ferromagnetic transition in VI_3 single crystals. We obtained critical exponents $\beta = 0.244(5)$ with a critical temperature $T_c = 50.10(2)$ K and $\gamma = 1.028(12)$ with $T_c = 49.97(5)$ K from the modified Arrott plot, whereas critical isotherm analysis resulted in $\delta = 5.24(2)$ at $T_c = 50$ K. This suggests that the ferromagnetic phase transition in VI_3 follows the tricritical mean-field model and that it is situated close to a two- to three-dimensional tricritical point. Furthermore, the magnetic entropy change $-\Delta S_M$ features a maximum at T_c , i.e., $-\Delta S_M^{max} \sim 2.64 \text{ J kg}^{-1} \text{ K}^{-1}$ with out-of-plane field change of 5 T. This is consistent with the $-\Delta S_M^{max} \sim 2.80 \text{ J kg}^{-1} \text{ K}^{-1}$ deduced from the heat capacity and the corresponding adiabatic temperature change $\Delta T_{ad} \sim 0.96$ K with out-of-plane field change of 5 T. The rescaled $\Delta S_M(T, H)$ curves collapse onto a universal curve, indicating a second-order type of the magnetic transition.

I. INTRODUCTION

Layered intrinsically ferromagnetic (FM) semiconductors hold great promise for both fundamental physics and applications in spintronic devices.^{1–5} CrI_3 has recently attracted much attention since the long-range magnetism persists in monolayer with T_c of 45 K.³ Intriguingly, the magnetism in CrI_3 is layer-dependent, from FM in monolayer, to antiferromagnetic (AFM) in bilayer, and back to FM in trilayer.³ In van der Waals (vdW) heterostructures formed by an ultrathin CrI_3 and a monolayer WSe_2 , the WSe_2 photoluminescence intensity strongly depends on the relative alignment between photoexcited spins in WSe_2 and the CrI_3 magnetization.⁶ Furthermore, the magnetism in ultrathin CrI_3 could be controlled by electrostatic doping, providing great opportunities for designing magneto-optoelectronic devices.^{7,8} Recently, the two-dimensional (2D) ferromagnetism has also been predicted in VI_3 monolayer with a calculated T_c of 98 K, higher than that in CrI_3 .⁹

Bulk CrI_3 and VI_3 belong to a well-known family of transition metal trihalides MX_3 ($X = \text{Cl}, \text{Br}$ and I).^{10,11} When compared to CrI_3 , in which the chromium has a half filled t_{2g} level yielding $S = 3/2$, the vanadium in VI_3 has two valence electrons that half fill two of the three degenerate t_{2g} states yielding $S = 1$.^{12–14} Bulk VI_3 is an insulating 2D ferromagnet with $T_c = 55$ K that crystallizes in a layered structure of BiI_3 with space group $R\bar{3}$ below 79 K whereas at higher temperatures VI_3 adopts layered monoclinic $C2/m$ crystal structure with van der Waals bonds along the c -axis.^{14–17} Density functional theory (DFT) calculations suggest that the VI_3 not only hosts the long-range ferromagnetism down to a monolayer but also exhibits Dirac half-metallicity, of interest for spintronic applications.⁹

The magnetocaloric effect (MCE) in the FM vdW materials gives additional insight into the magnetic properties. Bulk CrI_3 exhibits anisotropic $-\Delta S_M^{max}$ with values of 4.24 and 2.68 $\text{J kg}^{-1} \text{ K}^{-1}$ at 5 T for $\mathbf{H} // \mathbf{c}$ and $\mathbf{H} // \mathbf{ab}$, respectively,¹⁸ however little is known about VI_3 .

In the present work we focus on the nature of the FM transition in bulk VI_3 single crystals. We have investigated the critical behavior by the modified Arrott plot and a critical isotherm analysis, whilst the magnetocaloric effect was studied by the heat capacity and magnetization measurements near T_c . Critical exponents $\beta = 0.244(5)$ with $T_c = 50.10(2)$ K, $\gamma = 1.028(12)$ with $T_c = 49.97(5)$ K, and $\delta = 5.24(2)$ at $T_c = 50$ K, suggest that the magnetic transition is second-order and that it is situated near a tricritical point from two- to three-dimensional. This is further confirmed by the scaling analysis of magnetic entropy change $-\Delta S_M(T, H)$, in which the rescaled $-\Delta S_M(T, H)$ collapse on a universal curve independent on temperature and field.

II. EXPERIMENTAL DETAILS

Bulk VI_3 single crystals were fabricated by chemical vapor transport method starting from an intimate mixture of vanadium powder (99.95 %, Alfa Aesar) and anhydrous iodine beads (99.99 %, Alfa Aesar) with a molar ratio of 1 : 3. The starting materials were sealed in an evacuated quartz tube and then placed inside a multi-zone furnace. Materials were reacted over a period of 7 days with source zone at 650 °C, middle growth zone at 550 °C, and third zone at 600 °C. The x-ray diffraction (XRD) data were taken with $\text{Cu K}\alpha$ ($\lambda = 0.15418$ nm) radiation of Rigaku Miniflex powder diffractometer. The element analysis was performed using an energy-dispersive x-ray spectroscopy in a JEOL LSM-6500 scanning electron microscope, confirming a stoichiometric VI_3 single crystal. The magnetization data as a function of temperature and field were collected using Quantum Design MPMS-XL5 system in temperature range from 10 to 90 K with a temperature step of 1 K around T_c and field up to 5 T. The applied field (H_a) has been corrected for the internal field as $H = H_a - NM$, where M is the measured magnetization and N is the demagnetization factor. The corrected H was used for the analysis

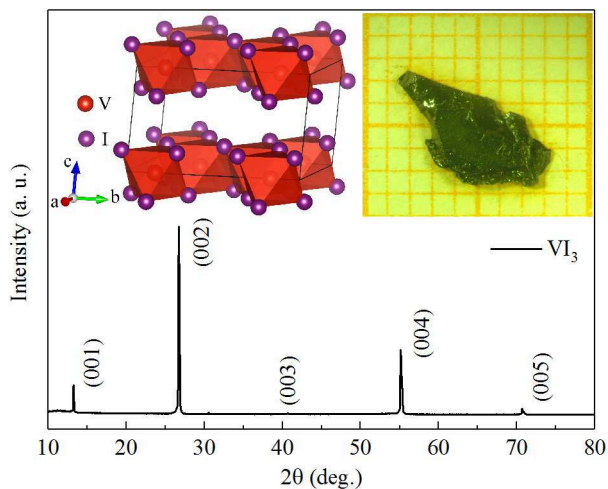


FIG. 1. (Color online) Single crystal x-ray diffraction pattern of VI_3 at room temperature. Inset shows the crystal structure and representative single crystal.

of the critical behavior. The magnetic entropy change $-\Delta S_M$ from the magnetization data was estimated using a Maxwell relation.

III. RESULTS AND DISCUSSIONS

The crystal structure of VI_3 forms in monoclinic AlCl_3 type with space group $C2/m$ at room temperature [inset in Fig. 1],^{12–14} similar to that of CrI_3 . The V ions are arranged in a honeycomb network and are located at the centers of distorted edge-sharing octahedra of six I anions. The I-V-I triple layers of composition VI_3 are stacked along the c axis and there are vdW gaps between them. The as-grown single crystals are shiny black platelets with lateral dimensions up to several millimeters, as shown in the inset of Fig. 1. In the single-crystal x-ray diffraction (XRD) scan [Fig. 1], only $(00l)$ peaks are detected, indicating that the crystal surface is normal to the c axis with the plate-shaped surface parallel to the ab plane.

Figures 2(a) and 2(b) present the temperature dependence of dc magnetic susceptibility measured in the fields ranging from 100 Oe to 50 kOe applied in the ab plane and along the c axis, respectively. It can be clearly seen that VI_3 exhibits a ferromagnetic transition at low temperature for both field directions. The magnetic susceptibility is nearly isotropic in 10 and 50 kOe, however, significant magnetic anisotropy is observed in 100 Oe and 1 kOe at low temperature. When $T < T_c$, the divergence of zero-field cooling (ZFC) and field-cooling (FC) curves exhibit a characteristic behavior of possible spin-glass or cluster-glass state with the temperature of divergence decreasing with increasing field. An additional weak anomaly at 80 K is also observed for $\mathbf{H} // \mathbf{c}$, which is field-independent. A structural phase transition accompanies similar feature in the susceptibility of CrI_3 ,²

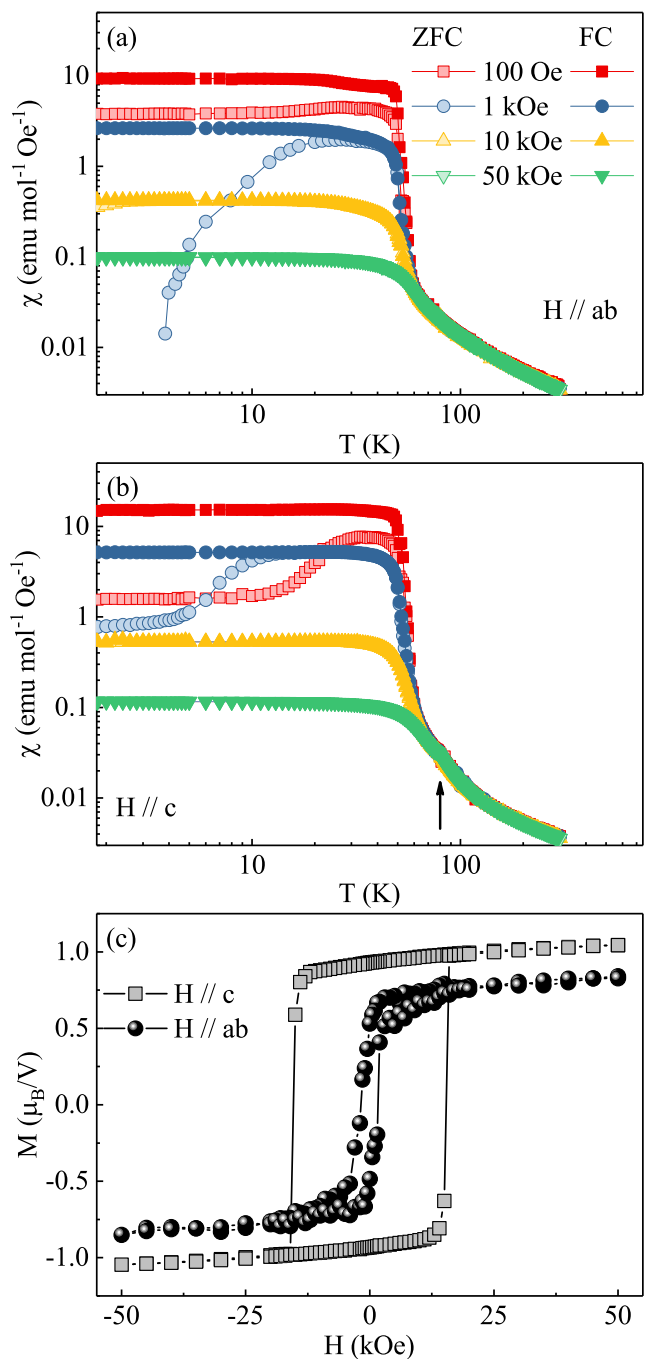


FIG. 2. (Color online) Temperature dependence of dc magnetic susceptibility χ for VI_3 measured in various magnetic fields applied (a) in the ab plane and (b) along the c axis, respectively. (c) Field dependence of magnetization measured at $T = 2$ K.

indicating strong spin-lattice coupling. Isothermal magnetization at $T = 2$ K [Fig. 2(c)] shows saturation moments of $M_s \approx 0.72 \mu_B/\text{V}$ and $0.95 \mu_B/\text{V}$ for $\mathbf{H} // \mathbf{ab}$ and $\mathbf{H} // \mathbf{c}$, respectively. The coercive field is about 15 kOe for $\mathbf{H} // \mathbf{c}$, much larger than that of around 1.5 kOe for $\mathbf{H} // \mathbf{ab}$. Both are significantly larger than those in

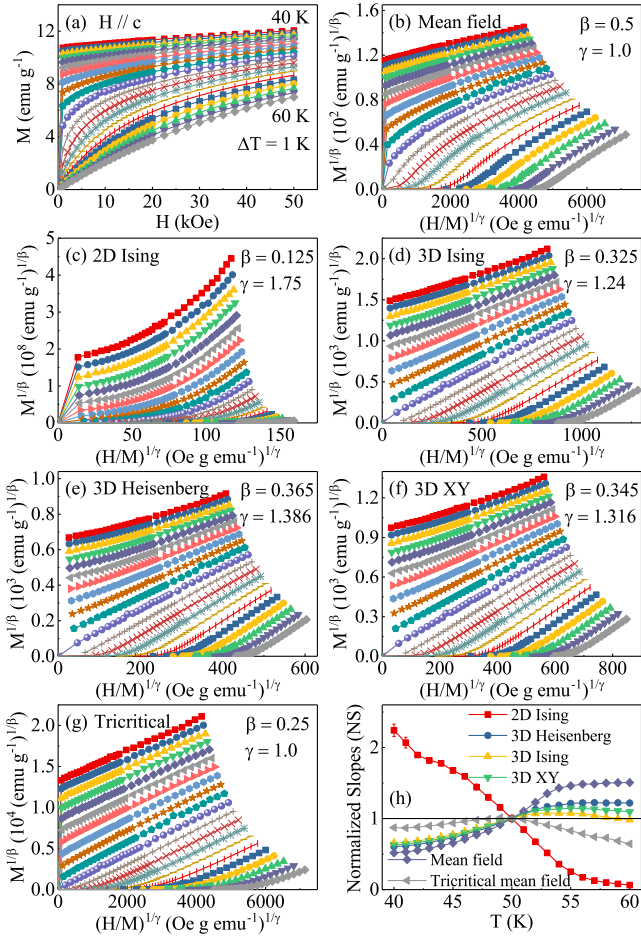


FIG. 3. (Color online) (a) Typical initial isothermal magnetization curves measured in out-of-plane fields from 40 to 60 K with a temperature step of 1 K for VI₃. (b) the Arrott plots of M^2 vs H/M . The $M^{1/\beta}$ vs $(H/M)^{1/\gamma}$ with parameters of (c) 2D Ising model, (d) 3D Ising model, (e) 3D Heisenberg model, (f) 3D XY model, and (g) tricritical mean-field model. (h) Temperature dependence of the normalized slopes $NS = S(T)/S(T_c)$ for different models.

CrI₃.¹⁹

Near T_c the second order phase transition is governed by magnetic equation of state and is characterized by critical exponents β , γ and δ that are mutually related.²⁰ Spontaneous magnetization M_s and inverse initial susceptibility χ_0^{-1} , below and above T_c can be used to obtain β and γ whereas δ is the critical isotherm exponent. Hence, from magnetization:

$$M_s(T) = M_0(-\varepsilon)^\beta, \varepsilon < 0, T < T_c, \quad (1)$$

$$\chi_0^{-1}(T) = (h_0/m_0)\varepsilon^\gamma, \varepsilon > 0, T > T_c, \quad (2)$$

$$M = DH^{1/\delta}, T = T_c, \quad (3)$$

where $\varepsilon = (T - T_c)/T_c$ is the reduced temperature, and M_0 , h_0/m_0 and D are the critical amplitudes.²¹

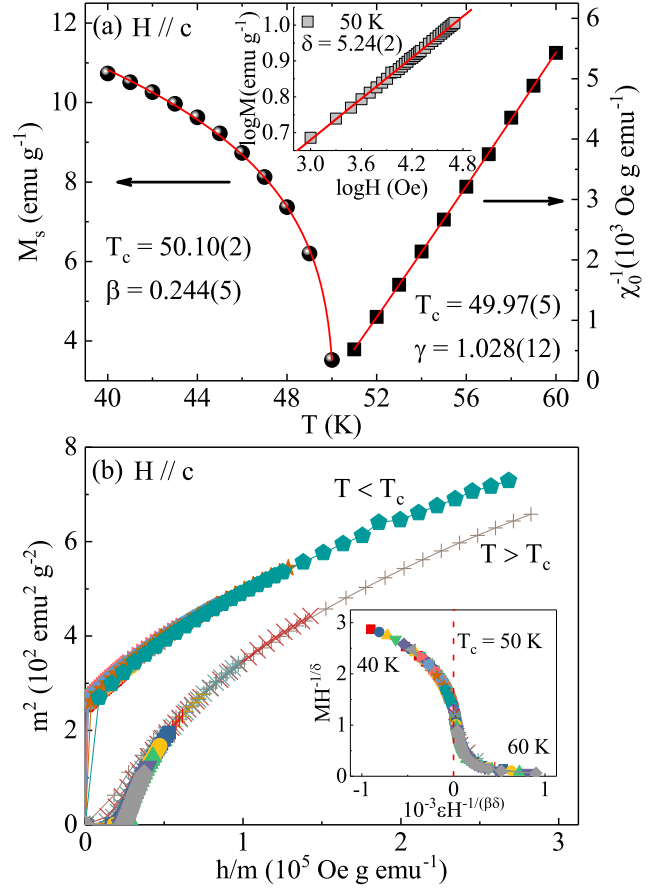


FIG. 4. (Color online) (a) Temperature dependence of the spontaneous magnetization M_s (left) and the inverse initial susceptibility χ_0^{-1} (right) with solid fitting curves. Inset shows the $\log M$ vs $\log H$ collected at 50 K with linear fitting curve. (b) Scaling plots of m^2 vs h/m with the scaled magnetization $m \equiv \varepsilon^{-\beta} M(H, \varepsilon)$ and the scaled field $h \equiv \varepsilon^{-(\beta+\gamma)} H$ below and above T_c for VI₃. Inset shows the rescaling of the $M(H)$ curves by $MH^{-1/\delta}$ vs $\varepsilon H^{-1/(\beta\delta)}$.

Isothermal magnetization in the temperature range from 40 to 60 K with a temperature step of 1 K is shown in Fig. 3(a). The Arrott plot involves mean-field critical exponents $\beta = 0.5$ and $\gamma = 1.0$.²² Based on this, magnetization isotherms M^2 vs H/M should be a set of parallel straight lines and the isotherm at the critical temperature T_c should pass through the origin. As shown in Fig. 3(b), all curves in the Arrott plot of VI₃ are nonlinear, with a downward curvature, demonstrating that the Landau mean-field model is not applicable to VI₃. However, it is possible to estimate the order of the magnetic transition through the slope of the straight line based on Banerjee's criterion.²³ First (second) order phase transition corresponds to negative (positive) slope. Therefore, the downward slope reveals a second-order PM-FM transition in VI₃.

Arrot-Noaks equation of state provides modification of

Arrot plot:²⁴

$$(H/M)^{1/\gamma} = a\varepsilon + bM^{1/\beta}, \quad (4)$$

where $\varepsilon = (T - T_c)/T_c$ and a and b are constants. The modified Arrot plots²⁵ [Figs. 3(c)-(g)] are obtained using possible exponents from 2D Ising ($\beta = 0.125, \gamma = 1.75$), 3D Ising ($\beta = 0.325, \gamma = 1.24$), 3D Heisenberg ($\beta = 0.365, \gamma = 1.386$), 3D XY ($\beta = 0.345, \gamma = 1.316$), and tricritical mean-field model ($\beta = 0.25, \gamma = 1.0$). The modified Arrott plot should be a set of parallel lines in the high field region with the same slope [$S(T) = dM^{1/\beta}/d(H/M)^{1/\gamma}$] for the correct model. The model which fits the data best is selected via normalized slope (NS), $NS = S(T)/S(T_c)$, that compares with the ideal value of unity. Plot of NS vs T for different models is presented in Fig. 3(h). It is clearly seen that the NS of 2D Ising model shows the largest deviation from unity. The NS of 3D Ising model is close to $NS = 1$ mostly above T_c , while that of tricritical mean field model is the best below T_c , suggesting a 3D magnetic behavior in bulk VI_3 .

The final and reliable values of M_s and H/M [solid line, Fig. 4(a)] are selected by linear extrapolation from the high field region to $M^{1/\beta}$ and $(H/M)^{1/\gamma}$ intercepts.²⁶ Critical exponents $\beta = 0.244(5)$, with $T_c = 50.10(2)$ K, and $\gamma = 1.028(12)$, with $T_c = 49.97(5)$ K, are obtained. According to Eq. (3), the $M(H)$ at T_c should be a straight line in log-log scale with the slope of $1/\delta$. As shown in the inset of Fig. 4(a), such fitting yields $\delta = 5.24(2)$. The Widom scaling law gives $\delta = 1 + \gamma/\beta$. From β and γ obtained with the modified Arrott plot, $\delta = 5.21(4)$, which is very close to that obtained from critical isotherm analysis.

Scaling analysis can be used to estimate the reliability of the obtained critical exponents and T_c . Near phase transition the magnetic equation of state is:

$$M(H, \varepsilon) = \varepsilon^\beta f_\pm(H/\varepsilon^{\beta+\gamma}), \quad (5)$$

where f_+ for $T > T_c$ and f_- for $T < T_c$, respectively, are the regular functions. Eq.(5) can be expressed via rescaled magnetization $m \equiv \varepsilon^{-\beta}M(H, \varepsilon)$ and rescaled field $h \equiv \varepsilon^{-(\beta+\gamma)}H$ as

$$m = f_\pm(h). \quad (6)$$

For the correct scaling relations and correct choice of β , γ , and δ , scaled m and h fall on universal curves above T_c and below T_c , respectively. Figure 4(b) presents the scaled m^2 vs h/m that collapse on two separate branches below and above T_c , respectively, confirming proper treatment of the critical regime. The scaling equation of state also takes another form

$$\frac{H}{M^\delta} = k\left(\frac{\varepsilon}{H^{1/\beta}}\right), \quad (7)$$

where $k(x)$ is the scaling function. From Eq. (7), all the experimental data should fall into a single curve. This

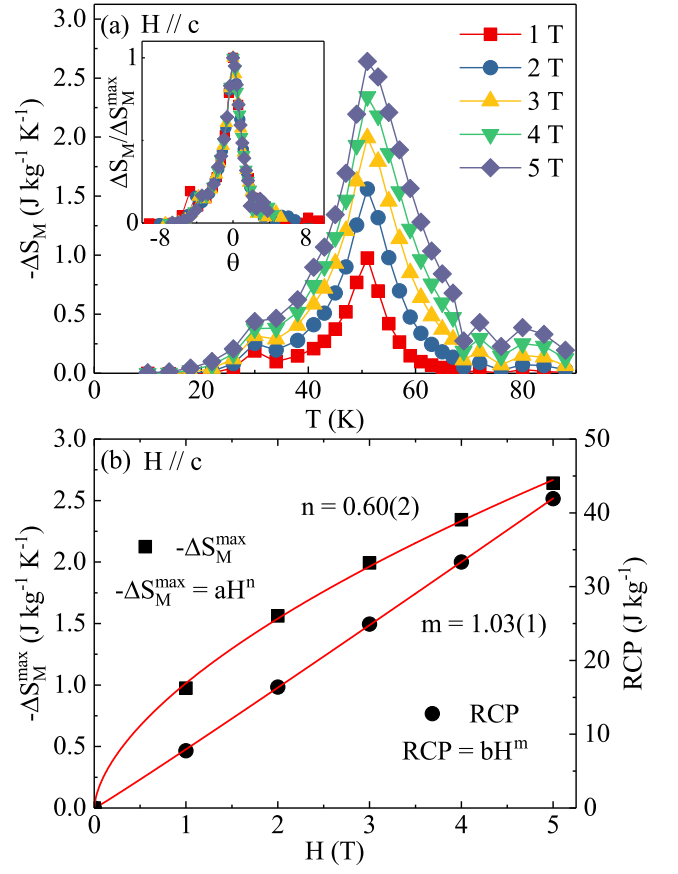


FIG. 5. (Color online) (a) The magnetic entropy change $-\Delta S_M$ obtained from magnetization at various out-of-plane field changes. Inset shows the normalized ΔS_M as a function of the rescaled temperature θ . (b) magnetic field dependence of the maximum magnetic entropy change $-\Delta S_M^{\max}$ and the relative cooling power RCP with power law fitting in red solid lines.

is indeed seen in the inset of Fig. 4(b); the $MH^{-1/\delta}$ vs $\varepsilon H^{-1/(\beta\delta)}$ experimental data collapse into a single curve and the T_c is located at the zero point of the horizontal axis.

The change of magnetic entropy is:

$$\Delta S_M(T, H) = \int_0^H \left[\frac{\partial S(T, H)}{\partial H} \right]_T dH. \quad (8)$$

This can be expressed using Maxwell's relation $\left[\frac{\partial S(T, H)}{\partial H} \right]_T = \left[\frac{\partial M(T, H)}{\partial T} \right]_H$ as:²⁷

$$\Delta S_M(T, H) = \int_0^H \left[\frac{\partial M(T, H)}{\partial T} \right]_H dH. \quad (9)$$

For magnetization measured at small (H, T) intervals, $\Delta S_M(T, H)$ is becomes:

$$\Delta S_M(T_i, H) = \frac{\int_0^H M(T_i, H) dH - \int_0^H M(T_{i+1}, H) dH}{T_i - T_{i+1}}. \quad (10)$$

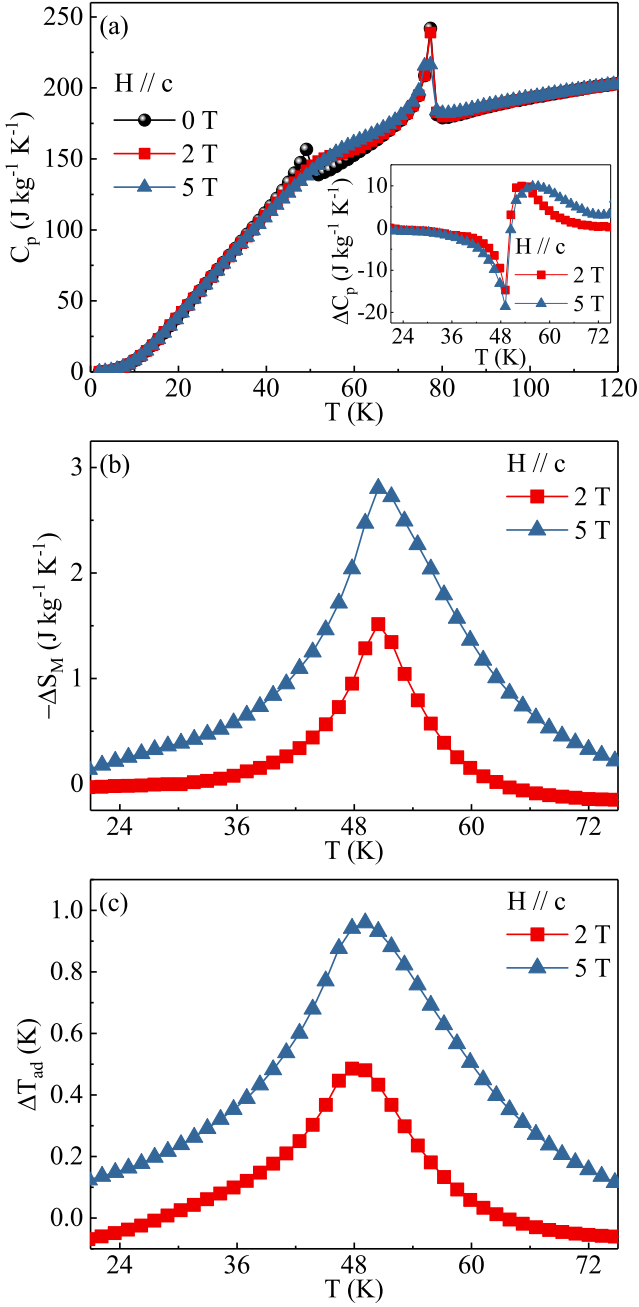


FIG. 6. (Color online) Temperature dependence of (a) the specific heat C_p , (b) the magnetic entropy change $-\Delta S_M$, and (c) the adiabatic temperature change ΔT_{ad} for VI_3 at the indicated out-of-plane fields. Inset in (a) shows the temperature-dependent specific heat change ΔC_p .

Figure 5(a) gives the calculated $-\Delta S_M$ as a function of temperature. All the $-\Delta S_M(T, H)$ curves exhibit a pronounced peak at T_c , and the peak broadens asymmetrically on both sides with increasing field. The maximum value of $-\Delta S_M$ reaches $2.64 \text{ J kg}^{-1} \text{ K}^{-1}$ with out-of-plane field change of 5 T.

$-\Delta S_M$ scaling is assessed from normalizing all the $-\Delta S_M$ curves against their maxima $-\Delta S_M^{max}$, i.e. ,

$\Delta S_M / \Delta S_M^{max}$ by temperature θ rescaling based on:²⁸

$$\theta_- = (T_{peak} - T) / (T_{r1} - T_{peak}), T < T_{peak}, \quad (11)$$

$$\theta_+ = (T - T_{peak}) / (T_{r2} - T_{peak}), T > T_{peak}, \quad (12)$$

where T_{r1} and T_{r2} are the temperatures of the two reference points that have been selected as those corresponding to $\Delta S_M(T_{r1}, T_{r2}) = \Delta S_M^{max} / 2$. It can be seen that the $-\Delta S_M(T, H)$ in different magnetic fields fall on a single line near T_c [inset in Fig. 5(b)].

At a second-order transition,²⁹ maximal magnetic entropy change can be expressed as $-\Delta S_M^{max} = aH^n$.³⁰ The relative cooling power (RCP) is defined: $RCP = -\Delta S_M^{max} \times \delta T_{FWHM}$. Here $-\Delta S_M^{max}$ is the maximum entropy change around T_c whereas δT_{FWHM} is the full-width at half maximum.³¹ The RCP changes in magnetic field as with $RCP = bH^m$. Figure 5(b) presents the summary of the out-of-plane field dependence of $-\Delta S_M^{max}$ and RCP. The calculated value of RCP is about 42 J kg^{-1} for VI_3 with out-of-plane field change of 5 T. Fitting of the $-\Delta S_M^{max}$ and RCP give that $n = 0.60(2)$ and $m = 1.03(1)$ for VI_3 .

The $-\Delta S_M$ can also be obtained from the heat capacity measurement with out-of-plane fields up to 5 T. The signature of magnetic order at $T_c = 50 \text{ K}$ in $H = 0$ [Fig. 6(a)] is suppressed in fields. Heat capacity change $\Delta C_p = C_p(T, H) - C_p(T, 0)$ [Fig. 6(a)] is $\Delta C_p < 0$ for $T < T_c$ and $\Delta C_p > 0$ for $T > T_c$. At T_c there is a sharp change from negative to positive. In contrast, the sharp peak at higher temperature ($\sim 80 \text{ K}$) is insensitive to external field and there is almost no shift when the field is up to 5 T. This heat capacity anomaly corresponds to the structural transition, in line with the magnetic susceptibility anomaly, indicating strong spin-lattice coupling in VI_3 . The entropy $S(T, H)$ can be deduced by

$$S(T, H) = \int_0^T \frac{C_p(T, H)}{T} dT. \quad (13)$$

Assuming the electronic and lattice contributions are not field dependent and in an adiabatic process of changing the field, the magnetic entropy change $-\Delta S_M$ can be straightly obtained $-\Delta S_M(T, H) = S_M(T, H) - S_M(T, 0)$. The adiabatic temperature change ΔT_{ad} caused by the field change can be obtained by $\Delta T_{ad}(T, H) = T(S, H) - T(S, 0)$, where $T(S, H)$ and $T(S, 0)$ are the temperatures in the field $H \neq 0$ and $H = 0$, respectively, at constant total entropy $S(T, H)$. Figures 6(b) and 6(c) show the temperature dependence of $-\Delta S_M$ and ΔT_{ad} estimated from heat capacity with out-of-plane field. The maxima of $-\Delta S_M$ and ΔT_{ad} increase with increase field and reach the values of $2.80 \text{ J kg}^{-1} \text{ K}^{-1}$ and 0.96 K , respectively, with the field change of 5 T.

IV. CONCLUSIONS

In summary, we have studied the critical behavior and magnetocaloric effect around the FM-PM transition in bulk VI_3 single crystal. The PM-FM transition in VI_3 is identified to be of the second order. The critical exponents β , γ , and δ estimated from the modified Arrott plot follow the tricritical mean-field model. Considering its ferromagnetism can be maintained upon exfoliating

bulk crystals down to a single layer, further investigation on the size-dependent properties is of interest.

ACKNOWLEDGEMENTS

This work was supported by the U.S. Department of Energy, Office of Basic Energy Sciences as part of the Computation Material Science Program through the Center for Computational Material Spectroscopy and Design.

-
- ¹ M. A. McGuire, G. Clark, S. KC, W. M. Chance, G. E. Jellison, Jr., V. R. Cooper, X. D. Xu, and B. C. Sales, *Phys. Rev. M* **1** 014001 (2017).
- ² M. A. McGuire, H. Dixit, V. R. Cooper, and B. C. Sales, *Chem. Mater.* **27**, 612 (2015).
- ³ B. Huang, G. Clark, E. Navarro-Moratalla, D. R. Klein, R. Cheng, K. L. Seyler, D. Zhong, E. Schmidgall, M. A. McGuire, D. H. Cobden, W. Yao, D. Xiao, P. Jarillo-Herrero, and X. D. Xu, *Nature* **546**, 270 (2017).
- ⁴ C. Gong, L. Li, Z. L. Li, H. W. Ji, A. Stern, Y. Xia, T. Cao, W. Bao, C. Z. Wang, Y. Wang, Z. Q. Qiu, R. J. Cava, S. G. Louie, J. Xia, and X. Zhang, *Nature* **546**, 265 (2017).
- ⁵ K. L. Seyler, D. Zhong, D. R. Klein, S. Guo, X. Zhang, B. Huang, E. Navarro-Moratalla, L. Yang, D. H. Cobden, M. A. McGuire, W. Yao, D. Xiao, P. Jarillo-Herrero, and X. D. Xu, *Nature Physics* **14**, 277 (2018).
- ⁶ D. Zhong, K. L. Seyler, X. Linpeng, R. Cheng, N. Sivadas, B. Huang, E. Schmidgall, T. Taniguchi, K. Watanabe, M. A. McGuire, W. Yao, D. Xiao, K.-M. C. Fu, and X. Xu, *Sci. Adv.* **3**, e1603113 (2017).
- ⁷ S. Jiang, L. Li, Z. Wang, K. F. Mak, and J. Shan, arXiv:1802.07355.
- ⁸ B. Huang, G. Clark, D. R. Klein, D. MacNeill, E. Navarro-Moratalla, K. L. Seyler, N. Wilson, M. A. McGuire, D. H. Cobden, D. Xiao, W. Yao, P. Jarillo-Herrero, and X. D. Xu, arXiv:1802.06979.
- ⁹ J. He, S. Ma, P. Lyu, and P. Nachtigall, *J. Mater. Chem. C* **4**, 2518 (2016).
- ¹⁰ D. Juza, D. Giegling, and H. Schäfer, *Zeitschrift für anorganische und allgemeine Chemie* **366**, 121 (1969).
- ¹¹ J. Dillon and C. Olson, *J. Appl. Phys.* **36**, 1259 (1965).
- ¹² S. Son, M. J. Coak, N. Lee, J. Kim, T. Y. Kim, H. Hamidov, H. Cho, C. Liu, D. M. Jarvis, P. A. C. Brown, J. H. Kim, C.-H. Park, D. I. Khomskii, S. S. Saxena, and J.-G. Park, arXiv:1812.05284.
- ¹³ T. Kong, K. Stolze, E. I. Timmons, J. Tan, D. Ni, S. Guo, Z. Yang, R. Prozorov, and R. J. Cava, arXiv:1812.05982.
- ¹⁴ S. Tian, J.-F. Zhang, C. Li, T. Ying, S. Li, X. Zhang, K. Liu, and H. Lei, arXiv:1812.06658.
- ¹⁵ J. Trotter and T. Zobel, *Zeitschrift für Kristallographie - Crystalline Materials* **123**, 1524 (1966).
- ¹⁶ L. L. Handy and N. W. Gregory, *J. Am. Chem. Soc.* **72**, 5049 (1950).
- ¹⁷ J. Wilson, C. Maule, P. Strange, and J. Tothill, *Journal of Physics C: Solid State Physics* **20**, 4159 (1987).
- ¹⁸ Y. Liu and C. Petrovic, *Phys. Rev. B* **97**, 174418 (2018).
- ¹⁹ Y. Liu, C. Petrovic, *Phys. Rev. B* **97**, 14420(2018).
- ²⁰ H. E. Stanley, *Introduction to Phase Transitions and Critical Phenomena* (Oxford U. P., London and New York, 1971).
- ²¹ M. E. Fisher, *Rep. Prog. Phys.* **30**, 615 (1967).
- ²² A. Arrott, *Phys. Rev. B* **108**, 1394 (1957).
- ²³ S. K. Banerjee, *Phys. Lett.* **12**, 16 (1964).
- ²⁴ A. Arrott, and J. Noakes, *Phys. Rev. Lett.* **19**, 786 (1967).
- ²⁵ J. C. LeGuillou, and J. Zinn-Justin, *Phys. Rev. B* **21**, 3976 (1980).
- ²⁶ A. K. Pramanik, and A. Banerjee, *Phys. Rev. B* **79**, 214426 (2009).
- ²⁷ J. Amaral, M. Reis, V. Amaral, T. Mendonc, J. Araujo, M. Sa, P. Tavares, J. Vieira, *J. Magn. Magn. Mater.* **290**, 686 (2005).
- ²⁸ V. Franco and A. Conde, *Int. J. Refrig.* **33**, 465 (2010).
- ²⁹ H. Oesterreicher and F. T. Parker, *J. Appl. Phys.* **55**, 4334 (1984).
- ³⁰ V. Franco, J. S. Blazquez, and A. Conde, *Appl. Phys. Lett.* **89**, 222512 (1984).
- ³¹ K. A. Gschneidner Jr., V. K. Pecharsky, A. O. Pecharsky, and C. B. Zimm, *Mater. Sci. Forum* **315-317**, 69 (1999).